FULL PAPER

New insights in copper binding to human islet amyloid: the contribution of metal complex speciation to reveal the polypeptide toxicity

Antonio Magrì,*[a] Diego La Mendola,*[b]Vincenzo Giuseppe Nicoletti,[c] Giuseppe Pappalardo,[a] Enrico Rizzarelli[a,d]

Abstract: Type 2 diabetes (T2D) is considered a potential threat on a global level. Recently, the T2D has been listed as misfolding disease like Alzheimer's and Parkinson's. disease. Human islet amyloid polypeptide (hIAPP) is a molecule co-secreted in pancreatic β cells and represents the main constituent of aggregated amyloid of found in individuals affected by T2D. Trace element serum level is significantly influenced during the development of diabetes. In particular, the dys-homeostasis of Cu^{2+} may adversely affect the course of the disease.

Conflicting results have been reported on the protective role played by complex species formed by Cu^{2+} with hIAPP or its peptide fragments *in vitro.* The histidine 18 represents the main binding site for the metal ion but contrasting results have been reported on other residues involved in metal coordination, in particular those towards the N- or the C-terminus. Sequences encompassing the regions 17-29 and 14-22 were used to discriminate between the two models of hIAPP coordination modes. Due to the poor solubility in water, their polyethylene glycol (Peg) derivatives were synthesized. A peptide fragment encompassing the 17-29 region of rat amylin (rIAPP) in which in position 18 the Arg residue was substituted by a His residue was also obtained to assess that the Peg moiety does not alter the peptide second structure. The complex species formed by Cu^{2+} with Ac-Peg-hIAPP(17-29)-NH_2, Ac-rIAPP(17-29)R18H-NH_2 and Ac-Peg-hIAPP(14-22)-NH_2 were studied by potentiometric titrations coupled with spectroscopic methods (UV-Vis, CD, EPR). The combined thermodynamic and spectroscopic approach allowed us to demonstrate that hIAPP is able to bind Cu^{2+} starting from His18 imidazole nitrogen atom toward the N-terminus domain. The stability constants of copper(II) complexes with Ac-Peg-hIAPP(14-22)-NH_2 were used to simulate the different experimental conditions in which the aggregate formation and oxidative stress of hIAPP has been reported. Speciation unveils: i) the protective role played by increased Cu^{2+} amount on the hIAPP fibrillary aggregation; ii) the effect of adventitious trace of Cu^{2+} present in PBS buffer and a reducing fluorogenic probe on H_2O_2 production attributed to the polypeptide alone.

[a]   Dr. A. Magrì, Dr. G. Pappalardo, Prof. E. Rizzarelli
        Consiglio Nazionale delle Ricerche
        Istituto di Biostrutture e Bioimmagini-
        Via P. Gaifami 18, 95126 Catania, (Italy)
        E-mail: leotony@unict.it
[b]   Prof. D. La Mendola
        Dipartimento di Scienze Farmaceutiche
        Università di Pisa
        Via Bonanno Pisano, 6, 56126 Pisa (Italy)
        E-mail: lamendola@farm.unipi.it
[c]   Prof. V. G. Nicoletti
        Dipartimento di Scienze Biomediche e Biotecnologiche
        Università degli Studi di Catania
        Viale A. Doria 6, 95125 Catania, (Italy)
[d]   Prof. E. Rizzarelli
        Dipartimento di Scienze Chimiche
        Università degli Studi di Catania
        Viale A. Doria 6, 95125 Catania, (Italy)

Introduction

Many protein domains and even entire proteins lack of well-defined secondary and tertiary structures. These proteins, named native unfolded,[1] intrinsically unstructured[2] or intrinsically disordered proteins (IDPs),[3] even though perfectly functional, are unable to fold spontaneously into stable, fixed, globular three-dimensional structures. They fold into distinct conformations, by interacting with different partners (other proteins, nucleic acids, small molecules, metal ions or membranes)[4-7] and thus playing important roles in cell signalling, transcription, translation and cell cycle regulation.[8-9]

Many of IDPs are involved in the so-called misfolded diseases or amyloidosis,[10-12] causing aggregation processes with loss of function and gain of toxicity. Typical example of intrinsically disordered sequences that can form amyloid is human islet amyloid polypeptide (hIAPP) also named amylin.[13]

This polypeptide hormone originates in the pancreatic β-cells and is co-secreted with insulin, playing a role in glycemic control;[14-15] it is associated with the pathogenesis of type II diabetes (T2D) in its aggregated and fibrillar form.[16-17]

Mature hIAPP is 37 residues in length (KCNTATCATQRLANFLVHSSNNFGAILSSTNVGSNTY-NH₂) and contains different functional domains:[18-19] i) the N-terminus (residues 1-19) which binds membrane and insulin; ii) the amyloidogenic central peptide sequence (residues 20-29); and iii) the C-terminus (residues 30-37) involved in self-association processes. An intramolecular disulfide bond between Cys2 and Cys7 and an amidated C-terminus characterize the native protein. The full-length hIAPP monomer can adopt various conformations, including unstructured coils, α-helices, long β-hairpins, and mixed α-helical and β-sheet conformations.[20-25] Model membranes are able to induce stable helical structures.[26-29]

IAPP sequence is highly conserved among mammalians; however, only IAPP from humans, primates, and cats are able to form amyloid fibrils, whereas IAPP from rodents (rIAPP) is not amyloidogenic.[30-31]

Each monomer involved in hIAPP oligomers is featured by a β-strand-loop-β-strand (U-bend) fold (Figure 1) encompassing two antiparallel β-strands connected by one turn [β-strand (Leu12-Val17)-turn (His18-Asn21)-β-strand (Phe-Tyr27)] in the misfolded protein. [32-35] A third β-strand is located between Asn31 and Tyr37.
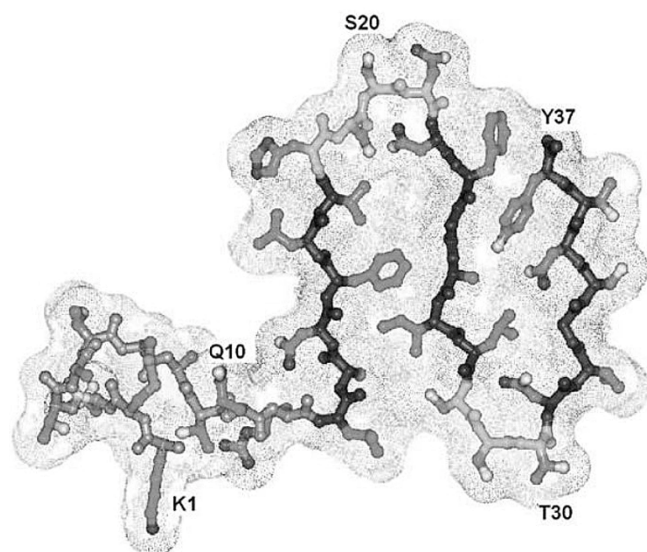

Figure 1: Proposed model of hIAPP in aggregated form. In black are reported the three β-strands cited in the text. (From Kajava et al. (ref. 33) with permission n° 3880121028167 obtained from Elsevier).

Rat IAPP (rIAPP) differs from hIAPP in only six amino acid residues, five are located within the 20-29 region (Figure 2).

Figure 2: Sequences of hIAPP and rIAPP, respectively. In the boxes are evidenced the differences of the two polypeptide.

There is a general agreement that the region 20-29 is aggressively amyloidogenic, while fragments 30-37 and 8-20 can contribute to form amyloid fibers.[36] However, the proline residues at positions 25, 28, and 29 reduce the amyloidogenic tendency of rIAPP.[31]

The sequence differences between human and mouse IAPP also include the substitution of His18 by Arg in mouse; though this residue does not belong to the amyloidogenic region, His18 plays a key role during the process of hIAPP aggregation and is involved in a complex H-bond network with the other residues around His18, including residues 15-21.[37-38]

The substitution of His with Arg in hIAPP(1-19)[39] can prevent the toxicity of this amylin fragment to alter the cellular membrane, probably caused by the charge of residue 18 and hIAPP(1-19) binds near the surface, similar to rat IAPP(1-19), at acidic pH when His-18 is protonated. [18, 39] The role played by the hIAPP histidine has further been reinforced by the findings of its involvement both in Zn^{2+} and Cu^{2+} interaction with the polypeptide and in the aggregate formation.[40-54]

Zn^{2+} can either favour[55] or inhibit[44-45] hIAPP aggregation; a link between ZnT8, an intracellular specific zinc transporter and type II diabetes (T2D) has also been suggested.[56]

Elevated serum Cu^{2+} levels have recently been associated with T2D [57-59] and the role of Cu^{2+} in the aggregation and dys-homeostasis of hIAPP is controversial.[53]

While some studies correlated the ability of Cu^{2+} to inhibit hIAPP fibrillation with toxicity,[46, 60] others pointed out that copper(II) may contribute to cytotoxicity by inducing hIAPP to form oligomers, which are more toxic to cells than fibrils.[54]

hIAPP-induced toxicity to β-cells was attributed to increased cellular ROS production [61] while copper (II) ion has been associated to the production of these toxic species and hIAPP amyloid aggregation.[49,53] However, the finding that the copper(II)-hIAPP complex produces hydrogen peroxide to a lesser extent than Cu^{2+}, may suggest a sacrificial protective role for IAPP in the presence of high copper amount.[48]
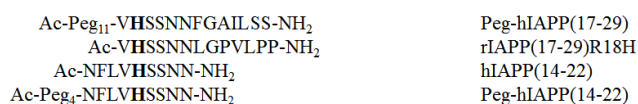
Further studies indicated an inhibitory role of copper(II) ion in human hIAPP and proIAPP amyloid aggregation,[51,62] including the ability of metal ion to induce a more compact conformation with no β-sheet folding.[41]

Different techniques have also been applied to elucidate the structure of copper(II)-hIAPP complexes and the putative binding sites[42, 50] in an attempt to correlate the structure of complex species with the Cu^{2+}-assisted aggregation inhibition of hIAPP and some of its peptide fragments.[40, 63]

However, there is a lack of study regarding the attribution of different structures of copper(II)-induced hIAPP aggregates to unique metal complexes that the polypeptide forms in the different experimental conditions. This aspect appears relevant to explain the controversial role played by copper(II) and zinc(II) as stressed by the recent findings showing that aggregation promotion or inhibition of hIAPP by the coordination of these metal depends on their concentrations.[48,64]

We employed the hIAPP(17-29) fragment and some Peg-conjugated peptides homologues to the hIAPP(17-29) [41, 65-67] as a model to study the effect of the environment (membrane, pH,

FULL PAPER

metal ion) on the aggregation process of the entire protein. In this study, we report on both the speciation of copper(II) complexes with different PEG-ylated peptide fragments of hIAPP and the metal coordination features of the different species formed at different copper(II) to peptide ratios, employing a combined potentiometric and spectroscopic approach. In particular, the copper(II) ion interaction with Peg-hIAPP(17-29), hIAPP(14-22), Peg-hIAPP(14-22) was investigated in detail. The Cu^{2+} complexes with rat-derived mutant rIAPP(17-29)R18H were also studied to verify if Peg chain derivatization could affect the complex formation and to determine the role of proline residues on the metal complex species structures. Finally, we also attempt to correlate the literature aggregation data with both the species formed in the reported experimental conditions (obtained by means of our speciation data) and their binding features. All the peptides are acetylated and amidated at N- and C- termini, respectively. Amino acid sequences and name abbreviations of the peptides used in the work are shown in Scheme 1.

Ac-Peg₁₁-VHSSNNFGAILSS-NH₂   Peg-hIAPP(17-29)
Ac-VHSSNNLGPVLPP-NH₂   rIAPP(17-29)R18H
Ac-NFLVHSSNN-NH₂   hIAPP(14-22)
Ac-Peg₄-NFLVHSSNN-NH₂   Peg-hIAPP(14-22)

Scheme 1: Amino acid sequences and name abbreviations of the four peptides used in this work. The different length of PEG chain was chosen to obtain soluble peptides with the minimal alteration of their conformations and chemical properties.

Results and Discussion

pH changes and Cu^{2+} affect Peg-hIAPP(17-29), rIAPP(17-29)R18H, hIAPP(14-22) and Peg-hIAPP(14-22) conformations.
The far UV-CD spectra of the un-complexed Peg-hIAPP(17-29) ligand have previously been carried out.[66] This Peg derivative showed a conformational switch from a random coil to a type II β-turn structure, upon histidine imidazole deprotonation (see Figure 1Sa).
Figure 3 shows the CD spectra recorded for the Peg-hIAPP(17-29) ligand in the presence of Cu^{2+} (molar ratio 1:1). At first sight, the Cu^{2+} addition does not differently affect the secondary region of the peptide in comparison to the pH change effects (Figure 3a).[66]
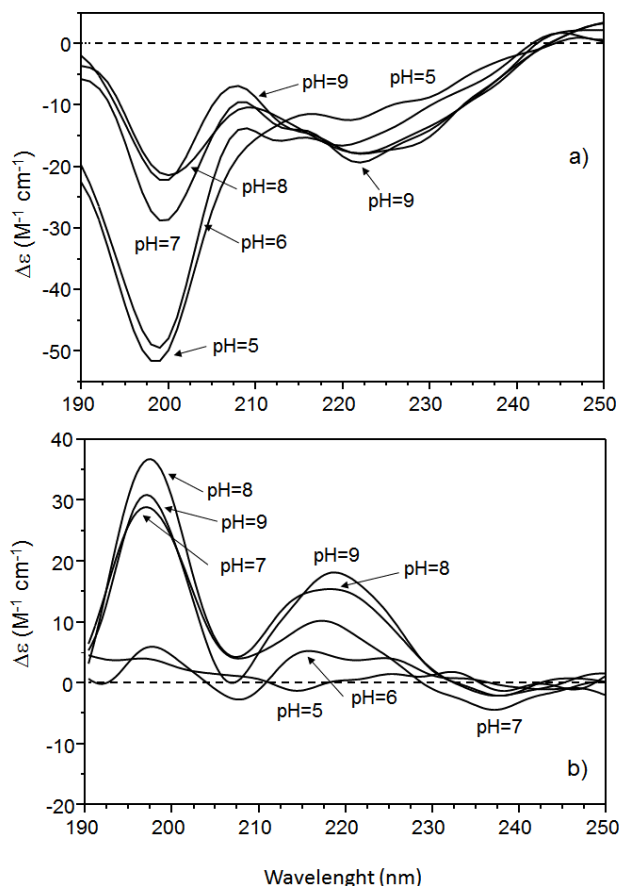

Figure 3: a) Far-UV CD spectra of Cu(II)-Peg-hIAPP(17-29) system and b) difference spectra between Cu(II)-Peg-hIAPP(17-29) and apo peptide. [L] = 5 × 10^{-5} mol dm^{-3}; molar ratio M:L = 1:1. Far UV CD spectra of apo peptide are reported in figure 1S(a). A colored version of this figure is reported in Supporting information section.

It induces the same conformational change from a random coil to a structured one, in the pH range 5-7, as indicated by the decrease of the negative ellipticity below 200 nm and the increase of the positive band around 208 nm, slightly shifted at longer wavelength with respect to the ligand alone. This can be due to the metal driven deprotonation of imidazole side-chain and it is indirect evidence that the histidine residue is the first anchoring site for Cu^{2+}. Increasing the pH, a strong decrease of minimum centered at 198 nm occurs together with a further red shift of the maximum at 208 nm and a wide band in the range 218-232 nm (Figure 3a). The apo-subtracted difference spectra show a maximum at 198 nm, a minimum at 207 nm and a maximum at 222 nm (Figure 3b). The first two signals are indicative of β-turn conformation whereas the maximum band at λ = 222 nm can be ascribed to the contribute of Phe residue aromatic ring in a ordered conformation as observed for other copper(II)-peptide systems.[68-70]
The copper(II) complex species induce a different conformational change in comparison with the β-turn type II observed for the free peptide in the pH range investigated.
The far-UV CD spectra of rIAPP(17-29)R18H are characterized by a strong negative band below λ = 200 nm, typical of peptides in a random-coil conformation, and a wide positive band around

225 nm, which suggests the contribution of type II polyproline component to the random-coil conformation of the peptide in all pH range 4-9 investigated. The CD spectra of apo peptide rIAPP(17-29)R18H are reported in Figure 1S(b).[65]

The spectrum of rIAPP(17-29)R18H changes upon addition of the metal ion, showing a reduction in the negative ellipticity with a slight red shift at λ = 200 nm, while a new negative band in the 220-230 nm range is evident increasing the pH (Figure 4a).
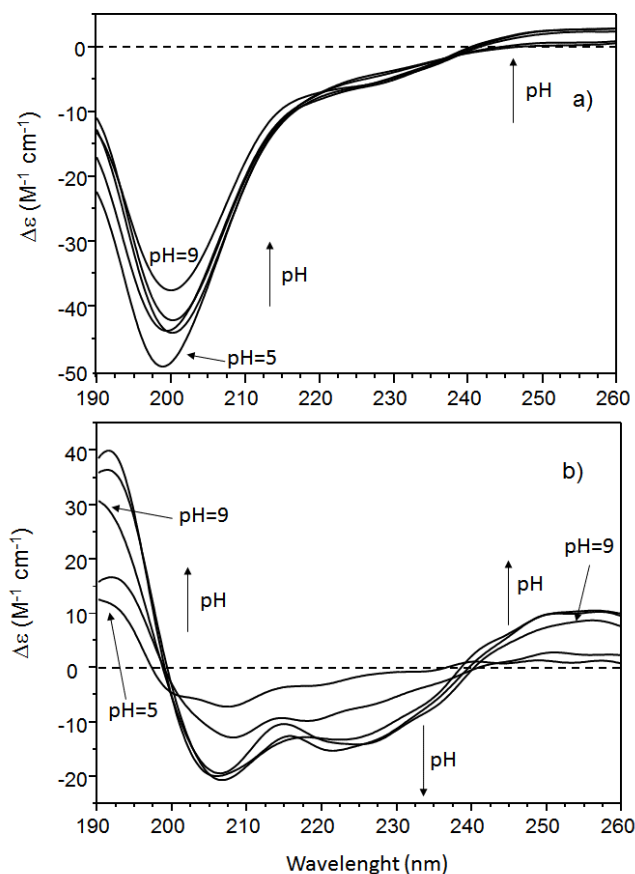

Figure 4: a) Far-UV CD spectra of Cu(II)-rIAPP(17-29)R18H system and b) difference spectra between Cu(II)-rIAPP(17-29)R18H and apo peptide. [L] = 5 × 10⁻⁵ mol dm⁻³; molar ratio M:L = 1:1. Far UV CD spectra of apo peptide are reported in figure 1S(b). A colored version of this figure is reported in Supporting information section.

Difference spectra, obtained by subtraction of the apo-peptide far-UV CD bands from those obtained in the presence of copper(II), gave a distinctive and well-defined CD-band profile in slightly acidic and basic pH, characterized by a positive band centered at λ = 192 nm, two negative bands centered at λ = 208 nm and λ = 224 nm, suggesting an α-helix secondary structure (Figure 4b).

The distribution diagram of the copper complexes with rIAPP(17-29)R18H (see next section) shows that, the histidine residue acts as metal-binding anchor to drive the deprotonation of amide nitrogen atoms which increase with the pH increase and favor a $1N_{im}$, xN^- (x = 1-4) binding mode for Cu^{2+}. Therefore, the difference spectra described above (Figure 4b) are indicative of conformational changes driven by amide coordination to Cu^{2+}.

To explore the ability of the His 18 to drive the copper(II) complex formation towards the N-terminus, the peptides hIAPP(14-22) and Peg-hIAAP(14-22) were synthesized. Their far-UV CD spectra display a minimum at around λ = 200 nm that decreases increasing the pH, while a slight maximum is found centered at λ = 215 nm, which increases and shifts at lower wavelength when the pH increases (Figure 2Sa and 2Sb). This aspect is typical of peptides in a random-coil conformation while the small maximum band centered at λ = 215 nm suggests the contribution of type II polyproline component.[71-72]

The pH changes do not significantly influence the band profile, though a shoulder at around λ = 225 nm is more evident increasing the pH. The peptide hIAPP(14-22) is soluble enough at the concentration range used to run the CD experiments. Interestingly, the band profile is similar to that of the PEG analogue, demonstrating that PEG conjugation does not introduce substantial differences to the conformational properties of the peptide chains. Moreover, CD experiments carried out at different metal/peptide ratios (pH 7.2) provide similar results for the two peptides (Figure 5a and 5b).
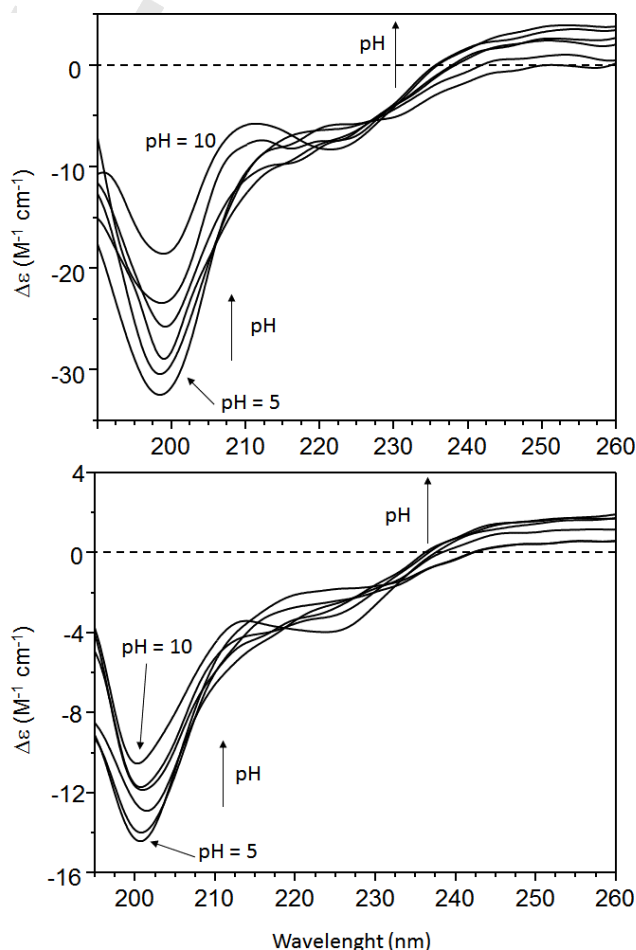

Figure 5: a) Far-UV CD spectra of Cu(II)-hIAPP(14-22) and b) and Cu(II)-Peg-hIAPP(14-22) systems, respectively. [L] = 5 × 10⁻⁵ mol dm⁻³; molar ratio M:L = 1:1 A colored version of this figure is reported in Supporting information section.

The copper addition to both peptide solutions induces CD spectra variations that appear pH dependent. The minimum at 198 nm decreases when the pH increases within the entire pH range investigated, the band profile at pH 10 shows a maximum centered at $\lambda = 208$ nm and a minimum at $\lambda = 220$ nm, while a shoulder appears between 215 and 220 nm in the pH 6-8 range (Figure 5a and 5b). The CD spectra suggest that the metal ion induces a structured conformation after pH 7, when the amount of free peptide is lower than that of metal complex species as indicated by the distribution diagram obtained in a 1 to 1 metal to peptide derivative (see next section). Difference spectra of both peptides encompassing the sequence 14-22, show a positive band centered at $\lambda = 192$ nm and a broad negative band centered at around $\lambda = 224$ nm (Figure 6a and 6b). It is interesting to note the difference with the analogous spectra obtained for the Peg-hIAPP(17-29): the red shift of both positive and negative band suggests the presence of β-turn structures rather than β-sheet. The peptide hIAPP(14-22) has not aromatic side chain and there is not a positive band at 222 nm, so this is an indirect proof of the phenylalanine side chain contribution in the Peg-hIAPP(17-29) spectra.
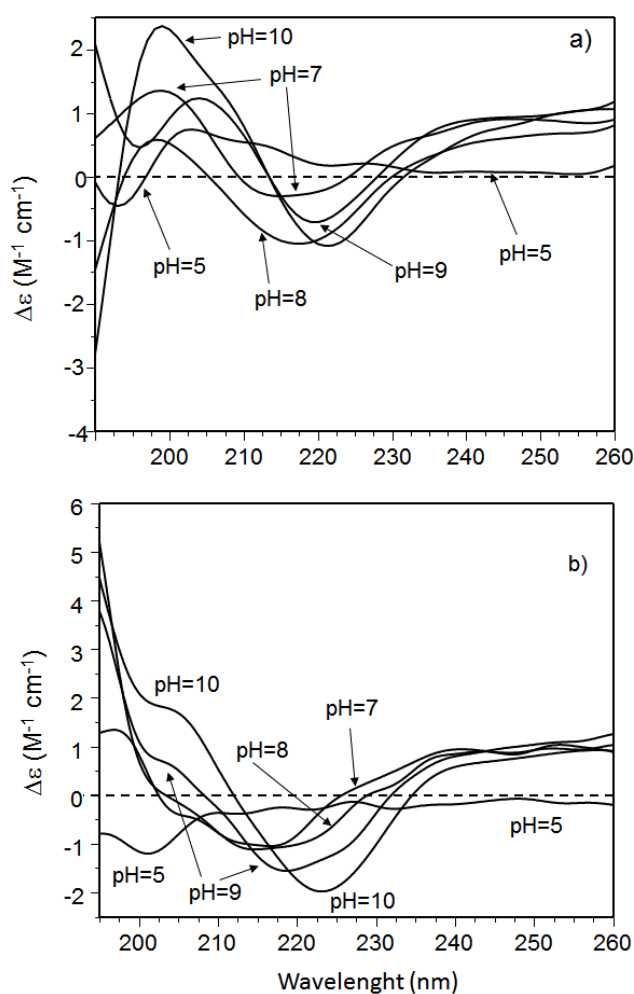

Figure 6: a) Difference spectra between Cu(II)-hIAPP(14-22) and apo peptide and b) difference spectra between Cu(II)-Peg-hIAPP(14-22) and apo peptide. A colored version of this figure is reported in Supporting information section.

Speciation, stability constants and coordination modes of Cu^{2+} with Ac-Peg-hIAPP(17-29) and rIAPP(17-29)R18H

Both Peg-hIAPP(17-29) and Ac-rIAPP(17-29)R18H peptides here investigated have only one protonation site. The protonation logβ values, reported in Table 1, are similar and in good agreement with those reported for analogous peptides containing only one histidine.[73]

Table 1. Stability constants (log β_{pqr}) for the proton and Cu(II) complexes with Peg-hIAPP(17-29), r-IAPP(17-29)R18H, Peg-hIAPP(14-22) (T= 298 K, I = 0.1 mol dm^{-3} KNO$_3$).[a]

Species	L= Peg-hIAPP(17-29) logβ_{pqr}	L= rIAPP(17-29)R18H logβ_{pqr}	L= Peg-hIAPP(14-22) logβ_{pqr}
[HL]	6.37 (2)	6.43 (1)	6.18 (1)
[CuL]	3.58 (3)	3.60 (5)	3.60 (5)
[CuLH$_{-1}$]	-2.79 (2)	-2.21 (2)	-
[CuLH$_{-2}$]	-8.88 (1)	-8.43 (2)	-8.31 (2)
[CuLH$_{-3}$]	-18.07 (3)	-17.58 (3)	-15.80 (2)
[CuLH$_{-4}$]	-28.03 (2)	-27.76 (3)	-24.71 (3)

[a]Standard deviations (3σ values) are given in parentheses. Charges are omitted for clarity.

The copper(II) complexes with the peptides were investigated at different metal to ligand molar ratios, 2:1, 1:1 and 1:2. The number of base equivalents consumed during the titration curves and the computer evaluation of the experimental data indicated that at 1:1 metal to peptide ratio, only mononuclear complexes were formed. The stability constant values of the Cu^{2+} complexes with the Peg-hIAPP(17-29) and rIAPP(17-29)R18H peptides are reported in Table 1. Species distribution diagram for copper(II) complex species with Peg-hIAPP(17-29) and rIAPP(17-29)R18H, are reported in Figure 7A and 7B, respectively.

The first species formed by both peptides is [CuL]. Taking into account that the peptides have N- and C- termini blocked by acetylation and amidation respectively, the anchoring site for copper(II) ion binding is the histidine imidazole nitrogen. The stability constant values are very similar for the two copper(II)-peptide systems and suggest the involvement of one imidazole nitrogen atom, as reported for similar systems.[68, 72]

EPR parameters for [CuL] formed by rIAPP(17-29)R18H (g$_{||}$ = 2.360, A$_{||}$ = 135 × 10^4 cm^{-1}), reported in Table 2, were obtained by subtraction of the free Cu^{2+} and confirm the presence of a CuN$_1$O$_3$ chromophore (N$_{im}$, 3O$_{water}$). On the contrary, it was not possible to get EPR parameters for the analogous complex species formed with Peg-hIAPP(17-29), due to the lower percentage formation. However, the UV-vis parameters (λ_{max} = 730 nm, ε = 30 M^{-1} cm^{-1}) obtained by means of titration experiments confirms the same coordination mode.
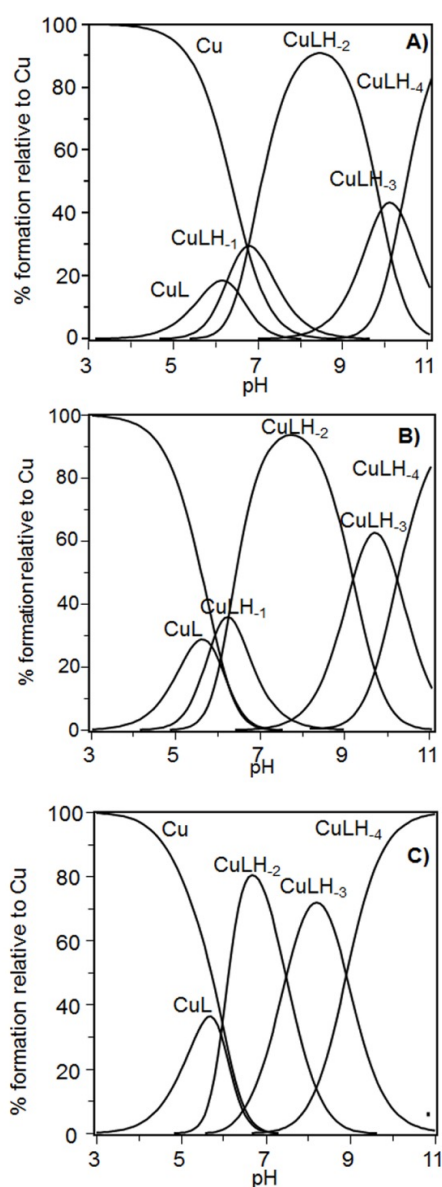
Figure 7: Species distribution diagram for copper(II) complex species with a) Peg-hIAPP(17-29) b) rIAPP(17-29)R18H and c) Peg-hIAPP(14-22). ([L] = [M] = 1 x 10^{-3} mol dm^{-3}).

Table 2. Spectroscopic parameters of copper(II) complexes with Peg-hIAPP(17-29), r-IAPP(17-29)R18H and Peg-hIAPP(14-22). ([L] = [M] = 1 × 10^{-3} mol dm^{-3}).

L	pH	Species (CuLH)	UV-vis λ (nm) (ε (M^{-1} cm^{-1}))	CD λ (nm) ($\Delta\varepsilon$ (M^{-1} cm^{-1}))	EPR $g_\parallel$	A$_\parallel$ (10^4 cm^{-1})
Peg-hIAPP(17-29)	6	Cu, [CuL], [CuLH$_{-1}$]	635	300 (-0.18); 617 (-0.29)	-	-
	7	[CuLH$_{-1}$], [CuLH$_{-2}$]	615	301 (-0.36); 340 (0.26); 606 (-0.79)	-	-
	8	[CuLH$_{-2}$]	605 (85)	304 (-0.05); 339 (0.27); 606 (-0.75)	2.225	161
	9	[CuLH$_{-2}$], [CuLH$_{-3}$], [CuLH$_{-4}$]	585	334 (0.24); 600 (-0.78)	-	-
	10	[CuLH$_{-2}$], [CuLH$_{-3}$], [CuLH$_{-4}$]	571	332 (0.21); 579 (-0.89)	-	-
	11	[CuLH$_{-4}$]	545 (98)	334 (0.14); 578 (-1.01)	2.189	203
r-IAPP(17-29)R18H	5.5	Cu, [CuL]	730 (30)	-	2.360	135
	6	Cu, [CuL], [CuLH$_{-1}$]	622	300 (-0.01); 336 (0.13); 607 (-0.29)	-	-
	7	[CuLH$_{-1}$], [CuLH$_{-2}$]	610	301 (-0.08); 337 (0.31); 611 (-0.76)	-	-
	8	[CuLH$_{-2}$]	601 (92)	304 (-0.01); 333 (0.29); 611 (-0.76)	2.223	153
	9	[CuLH$_{-2}$], [CuLH$_{-3}$]	585	331 (0.17); 594 (-0.66)	-	-
	10	[CuLH$_{-3}$], [CuLH$_{-4}$]	556	476 (0.08); 573 (-0.67)	-	-
	11	[CuLH$_{-4}$]	545 (101)	475 (0.12); 572 (-0.70)	2.195	201
Peg-hIAPP(14-22)	5.5	Cu, [CuL]	770 (25)	-	-	-
	6.5	[CuLH$_{-2}$]	617 (99)	493 (0.08); 625 (-0.67)	2.240	168
	7	[CuLH$_{-2}$], [CuLH$_{-3}$]	613	490 (0.04); 622 (-1.03)	-	-
	8	[CuLH$_{-3}$]	598 (130)	328 (0.10); 364 (-0.11); 611 (-0.86)	2.217	178
	9	[CuLH$_{-3}$], [CuLH$_{-4}$]	570	325 (0.27); 366 (-0.10), 589 (-0.80)	-	-
	11	[CuLH$_{-4}$]	536 (115)	325 (0.33); 370 (-0.05); 546 (-1.06)	2.104	206

Charges are omitted for clarity.

The CD spectra of the copper(II) complexes formed by Peg-hIAPP(17-29) and rIAPP(17-29)R18H below pH 6 show a low intensity d-d band in the visible region, confirming that the

copper(II) ion is mainly bound to donor atoms distant from chiral centres of peptide backbone.

The next complex [CuLH$_{-1}$] is a minor species and overlapped to other ones so its spectral parameters were not determined (see Figure 7A and 7B). Taking into account the pH range existence of [CuLH$_{-1}$], the coordination binding sites for the metal ion may involve the imidazole nitrogen and one deprotonated amide nitrogen.

In the pH range 6.5-9.0, [CuLH$_{-2}$] is the major species for both Cu(II)-Peg-hIAPP(17-29) and Cu(II)-rIAPP(17-29)R18H systems. The pK of the second amide deprotonation for Cu(II)-Peg-hIAPP(17-29) (logβ_{11-2} - logβ_{11-1} = 6.09; see table 1S) is lower than that of the first one. Such trend suggests that the deprotonation of first two amide nitrogen atoms is cooperative as reported for other copper(II)-peptides complexes.[69-70] (this trend was not observed for rIAPP(17-29)R18H). The spectroscopic parameters of [CuLH$_{-2}$] species are very similar for the two peptides suggesting a similar metal ion coordination environment. In the case of Cu(II)-Peg-hIAPP(17-29) system the CD spectrum carried out at pH 7.0 shows the presence of signals at 339 nm and at 304 nm clearly indicating the involvement in copper coordination of both imidazole and amide nitrogen atoms (Table 2). The UV-vis parameters (λ = 605 nm; ε = 85 M^{-1} cm^{-1}) are consistent with a 3N1O coordination mode in which one imidazole and two amide nitrogen atoms are coordinated to the metal ion. As reported for other copper(II) complexes with similar peptide fragments, the EPR parameters are consistent with a perturbation on the copper(II) in plane square coordination.[74-75]

The g$_\parallel$ values with a relatively low hyperfine coupling constants, particularly evident for the copper(II) complex species with rIAPP(17-29)R18H (g$_\parallel$ = 2.223, A$_\parallel$ = 153 × 10^{-4} cm^{-1}), indicate a tetrahedral distorted square-planar geometry even though a pyramidal square based stereochemistry cannot be ruled out.

Increasing the pH, the [CuLH$_{-3}$] is formed. It was not possible to determine spectroscopic parameters due to the overlapping with two major specie [CuLH$_{-2}$], [CuLH$_{-4}$] for both Peg-hIAPP(17-29) and rIAPP(17-29)R18H peptides. However, the blue-shift measured on λ_{max} in the pH range 9-10 (Table 2), clearly suggests the deprotonation of a third amide and a Cu^{2+} coordination mode involving one imidazole and three amide nitrogen atoms. In the CD spectrum, the N$^-$ → Cu^{2+} charge transfer is positive and overlaps to that of N$_{Im}$ charge transfer band so it is not possible to determine λ_{max}. The analogous copper(II) complex species with the mutated peptide rIAPP(17-29)R18H displays the same spectroscopic parameters which indicate a similar coordination environment. At very basic pH, another species [CuLH$_{-4}$] is formed. The blu-shift of UV-vis λ_{max}, and the EPR parameters (Table 2) indicate the deprotonation of another amide nitrogen, that replaces the imidazole nitrogen in the metal ion coordination environment. The low g$_\parallel$ value and the high hyperfine coupling constants indicate a planar disposition of donor atoms around Cu^{2+} as further confirmed by the decrease of molar adsorption coefficient.

Speciation, stability constants and coordination modes of Cu^{2+} with Ac-Peg-hIAPP(14-22)-NH$_2$

The peptide hIAPP(14-22) is not soluble at the millimolar concentrations required for the potentiometric measurements so it was not feasible to determine the stability constant values by means of this technique. However it is soluble at 5 × 10^{-4} mol dm^{-3} in all pH range investigated so it was possible to perform spectroscopic measurements in such experimental conditions. The conjugation with polyethylene glycol chain increased peptide solubility so to overcome this limit. As reported in Table 1, the histidine protonation constant of Peg-hIAPP(14-22) is slightly lower than that reported for the peptides encompassing the 17-29 amino acid residues but still in agreement with that reported for other peptides encompassing one histidine residue.[76]

In Table 1 are reported the stability constant values of the Cu^{2+} complexes with the Peg-hIAPP(14-22) whereas the distribution diagram is reported in Figure 7C.

The first copper(II) complex species formed is [CuL] that displays the same stability constant value (logβ = 3.60) measured for the other two investigated peptides. This finding suggests the presence of the same N$_{Im}$, 3O coordination environment. The next complex species is the [CuLH$_{-2}$] in which two amide nitrogen atoms are deprotonated. The pK value related to the two consecutive deprotonation step(logβ_{110} - logβ_{11-2} = 11.91) is slightly lower than that observed for Peg-hIAPP(17-29) and rIAPP(17-29)R18H ((logβ_{110} - logβ_{11-2} = 12.46 and 12.03, respectively). The UV-vis parameters extrapolated from the spectroscopic titrations are very similar to those obtained for hIAPP(14-22) peptide (data not shown), confirming again that the conjugation does not affect metal complexation. Such parameters (λ_{max} = 617 nm, ε = 99 M^{-1} cm^{-1}) indicate a 3N1O coordination mode with one imidazole and two amide nitrogen atoms bound to metal ion, suggesting a slight higher distortion in comparison to copper complexes with Peg-hIAPP(17-29) and rIAPP(17-29)R18H. The CD spectra carried out in the 6.5-7 pH range display two band in the d-d transition region and a wide band centred at 258 nm corresponding to the charge transfer π_{im} → Cu^{2+} that covers the signal related to N$^-$ → Cu(II) charge transfer. It is interesting to note that at physiological pH the [CuLH$_{-2}$] is the predominant species ($\approx$ 90%) for the two peptides encompassing the 17-29 amino acid residues (Figure 7A and 7B). In the case of Cu(II)-Peg-hIAPP(14-22) system, this complex species co-exists with the main species [CuLH$_{-3}$]. The third deprotonation step is highly favoured in this last system. This strong thermodynamic difference can be assigned to a different chelate ring formation indicating that the deprotonation step occurs towards the N-terminus for Peg-hIAPP(14-22) while it is obliged towards the C-terminus in the case of Peg-hIAPP(17-29) and rIAPP(17-29)R18H (see scheme 2).
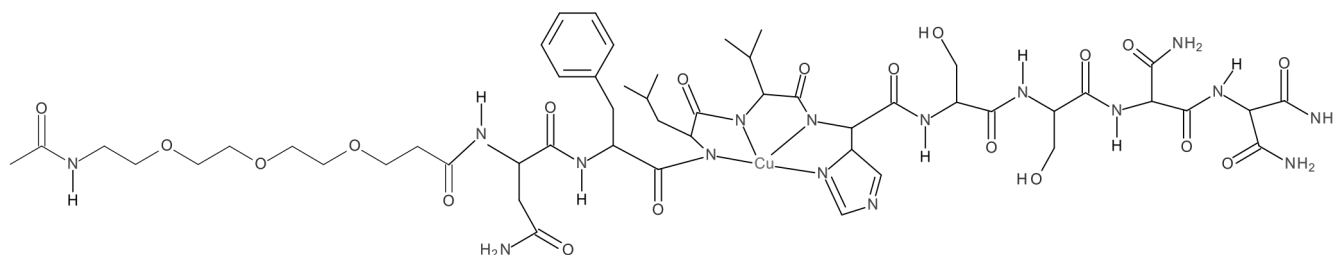
The UV-vis parameters (λ = 598 nm, ε = 130 M^{-1} cm^{-1}) for the [CuLH$_{-3}$] support a binding mode characterized by the increasing deprotonated amide nitrogen atoms, with a distortion of square-planar coordination geometry. In the CD spectrum carried out at pH 8, the bands related to the amide (328 nm) and imidazole charge transfers (258 nm and 364 nm) together with a large minimum band at 611 nm assigned to d-d transition, were observed. At higher pH values, a further deprotonation step occurs and pK$_{(-3-4)}$ value of 8.91 (see Table 1S) indicates the involvement of another amide nitrogen donor atom. The spectroscopic data indicate the involvement of four nitrogen atoms in plane with a strong equatorial field. The decrease of CD band related to imidazole charge transfer and the increase of amide nitrogen charge-transfer band, suggest that the nitrogen atoms in plane are those of the amide backbone. The λ_{max} value is lower than that obtained for the peptides encompassing the 17-29 amino acid residues whereas the ε values are higher, suggesting a strong ligand field in plane and a possible weak contribution of imidazole nitrogen in the axial position.

Speciation reveals the role of amino acid residues preceding histidine 18 in copper(II) binding

There is general agreement on the role of the histidine at position 18 in hIAPP as anchoring site for Cu^{2+} but an open question is represented by the other amino acid residues involved in metal binding, namely those that precede and follow the histidine residue located at position 18.[40]

To answer this question, we compared the thermodynamic and spectroscopic parameters of the copper(II) complexes with the peptides encompassing the 17-29 amino acid residues, with those of analogous species with the hIAPP(14-22) peptide fragment that includes additional residues towards the N-terminus for their involvement in metal binding. The distribution diagrams helped us to assess the specific spectroscopic parameters to individual species, starting from the basic pH where a single species forms though it was not relevant for biological aims. The [CuLH$_{-4}$] (L = Peg-IAPP(14-22)) shows different CD spectra features in comparison with those observed for analogous species formed by the two peptides which include the 17-29 amino acid sequence. The main d-d band is blue-shifted of 32 nm and the band intensity of the deprotonated nitrogen atom charge transfer is higher than the one of the imidazole. The EPR parameters indicate that Cu^{2+} experiences a similar coordination in terms of donor atoms (four nitrogens) but a slight different geometry and chiral environment. The distribution diagrams of the

different copper(II) complexes with the investigated peptides (Figure 7) show different pH values where the [CuLH$_{-2}$] represents the main and unique species; the maximum percentage of copper(II) complex formation is around pH 6.5 for L = Peg-hIAPP(14-22) and at pH 8 for the 17-29 peptides. The UV-vis parameters and the CD bands of the d-d transition pertinent to the two peptides containing the 17-29 amino acid residues are different from those related to the peptide encompassing the 14-22 amino acid residues (see Table 2) indicating that the copper coordination features are different, though the donor atom are equal, as indicated by EPR parameters. These differences strongly support a diverse role played by the amino acid residues preceding or following the His18 residue in the two couples of peptides. These conclusions are in agreement with previously reported thermodynamic data for copper(II) peptide systems[70] indicating the preference of the amide nitrogen deprotonation steps toward the N-terminus, due to the formation of the more stable [6+5] membered chelate rings in comparison to the [7+5] membered chelate rings when the C-termini residues are involved. Conversely, recent studies on different peptide fragments belonging to 15-29 region of the hIAPP, suggested that the deprotonation occurs towards the C-terminus involving residues His-18, Ser-19, Ser-20, Asn-21 and Asn-22.[40] This conclusion arises from data obtained with spectroscopic techniques (UV-Vis, CD, NMR and EPR). The results refer to pH 7.5 where the authors affirm that only one complex species of their copper(II)-h-IAPP(15-22) system is present. On the basis of our thermodynamic data and related distribution diagrams, their spectroscopic parameters belong to a mixture of [CuLH$_{-2}$] and [CuLH$_{-3}$] complex species as we found for the copper(II) complexes with the analogous peptide Peg-hIAPP(14-22) (see Figures 7). At pH 7.5 the [CuLH$_{-2}$] is the main species only for the peptides containing the 17-29 amino acid residues. The lack of speciation data seems to affect their NMR results, utilized to support their conclusion that the C-terminus is involved in the amide deprotonation. In fact, their NMR measurements have been carried out at 0.3:1 metal: peptide molar ratio (peptide concentration = 5 × 10^{-4} mol dm^{-3}); but in this experimental conditions our simulation results show (Figure 8) that the un-complexed peptide is the prevailing species (around 75%); some doubt, therefore, can arise on the reliability of the reported conclusion.

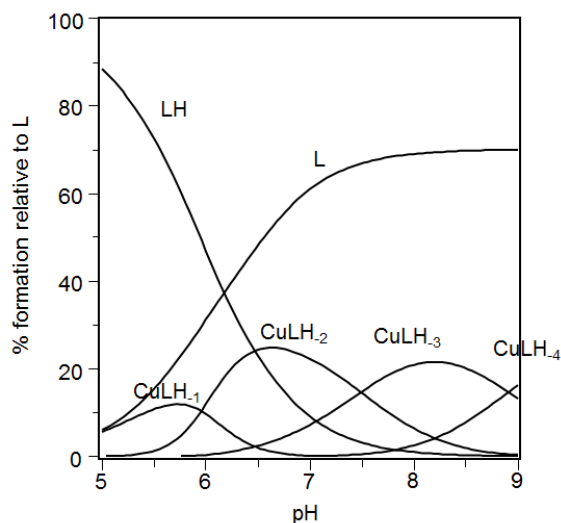**Scheme 2**: Schematic view of [CuLH$_{-3}$] complex species formed by Cu^{2+} and Peg-hIAPP(14-22).

Figure 8: Distribution diagram of Cu(II)-Peg-hIAPP(14-22) system reported respect to ligand. [L]= 5×10^{-4} mol dm^{-3}; M : L ratio 0.3:1.

The EPR measurements have been carried out at low temperature and then the speciation may be slightly different with respect to that obtained at room temperature. However, the EPR parameters ($g_{\parallel}$ = 2.236, $A_{\parallel}$ = 168 $\times$ 10^{-4} cm^{-1}) reported by Rivillas-Acevedo et al.[40] are quite similar to the species [CuLH$_{-2}$] obtained for Ac-Peg-hIAPP(14-22) ($g_{\parallel}$ = 2.240, $A_{\parallel}$ = 168 x 10^{-4} cm^{-1}) which are slightly different from those obtained for the Peg-hIAPP(17-29) ($g_{\parallel}$ = 2.225, $A_{\parallel}$ = 161 $\times$ 10^{-4} cm^{-1}) and rIAPP(17-29)R18H ($g_{\parallel}$ = 2.223, $A_{\parallel}$ = 151 $\times$ 10^{-4} cm^{-1}). In particular the hyperfine coupling constant is lower for these last two systems and similar to that reported for peptide having a proline located next to histidine residue at the N-terminus portion in analogy to the prion peptide fragments where the deprotonation processes occur necessarily towards the C-terminus.[74-77]

Speciation unveils both the protective role of increasing Cu^{2+} concentration on the hIAPP aggregate formation and the oxidative contribution of adventitious trace of copper(II) on H$_2$O$_2$ production caused by the polypeptide alone.

Elevated serum concentration and altered impaired copper metabolism occur in diabetes, playing specific roles in the pathogenesis and progression of the diabetic complications, including amyloidosis.[57-58,78]

The precise impact of this metal ion on IAPP aggregate formation is still a matter of debate;[41,79] according to cell-free studies, copper: i) can inhibit,[46,48-49] ii) does not modify hIAPP fibril formation,[53] or iii) can favour the accelerated low-molecular-weight oligomer granular formation, responsible of higher cytotoxicity than fibrils.[54]

In an early study, Allsop et al. reported that incubating CuCl$_2$ (1 $\times$ 10^{-5} mol dm^{-3}) with hIAPP (1 $\times$ 10^{-4} mol dm^{-3}) at pH = 7.4 (0.1 mol dm^{-3} of 4-(2-hydroxyethyl)-1-piperazineethanesulfonic acid, (HEPES) as buffer), did not change electron microscopy (EM) and atomic force microscopy (AFM) images of the hIAPP short protofibrils or longer amyloid fibrils (after prolonged incubation periods). [53]

In another recent study, copper(II) ion-induced hIAPP aggregation has been investigated by high-resolution transmission electron microscopy (HRTEM) and AFM.[54] The morphology of hIAPP aggregates changed by copper addition ([hIAPP] = 2 $\times$ 10^{-5} mol dm^{-3} and [Cu^{2+}] = 1 $\times$ 10^{-5} mol dm^{-3}), while Thioflavin (ThT) fluorescence assay and Tyrosine Intrinsic fluorescence assay results showed that hIAPP (1 $\times$ 10^{-5} mol dm^{-3}) fibrillogenesis was inhibited by copper in a metal concentration dependent manner. The inhibition increased with the increase of Cu^{2+} to peptide ratio (the inhibition percentages changed up to a metal to peptide ratio lower than 2). Furthermore, CD results indicated that Cu^{2+} not only affected the kinetics of hIAPP aggregation inhibiting fibril formation, but its binding to hIAPP also changed the peptide conformation.[54]

According to these results, the proposed mechanism suggested that i) copper accelerated small granular oligomer formation, and ii) copper-induced hIAPP cytotoxicity was due mainly to the formation of small granular oligomers of hIAPP rather than to ROS-mediated cytotoxicity, as suggested by Allsop in a previous work.[53]

Conversely, the results of ThT-assay and Intrinsic fluorescence assay indicated the inhibition of hIAPP fibrillogenesis ([hIAPP] = 4 $\times$ 10^{-7} mol dm^{-3}) by copper addition (1 $\times$ 10^{-5} mol dm^{-3}) at pH 7.4 (piperazine-N,N'-bis(2-ethanesulfonic) acid (PIPES) as buffer). [46] Cu^{2+} displayed a modulatory anti-aggregative properties in standard Th-T assay at a 1:1 metal to hIAPP ratio in phosphate buffer, accompanied by a sacrificial quenching of metal-catalyzed ROS by human hIAPP.[48]

Our stability constant values here determined and reported in Table 1 were used to determine the metal speciation of copper(II) complexes with IAPP in the experimental conditions reported in the above cited works.[46, 48] This approach allowed us to simulate the hIAPP related species and to explain the contrasting results on the role of metal ion in hIAPP aggregate formation.

According to the species distribution diagram shown in Figure 9, that simulates the conditions where the peptide to copper ratio is lower than 1:1, the main species at pH 7 results to be the free peptide.

This finding is consistent both with the EM and AFM data,[53] showing that IAPP fibril formation is not perturbed by adding copper (1 $\times$ 10^{-5} mol dm^{-3}) in the 1 $\times$ 10^{-4} mol dm^{-3} peptide solution and with the data obtained with the similar techniques[49 54] where the experimental condition are equal to those simulated by the speciation reported in Figure 9A.

The unbound peptide turns a minor species when the Peg-hIAPP(14-22) and the metal ion are present at the same molar equivalent (Figure 9B), while at pH 7.0 in the conditions where the metal ion to peptide ratio is 2:1, the distribution diagram clearly shows that the peptide is entirely bound and forms different copper(II) complex species (Figure 9C).
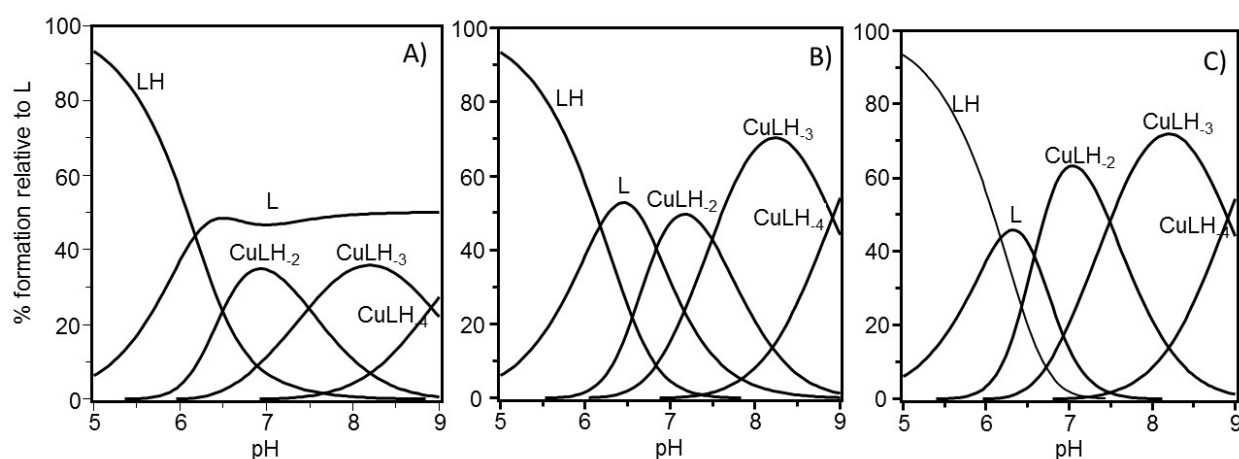
Figure 9: Distribution diagram of copper(II)-Peg-hIAPP(14-22) system reported respect to ligand. A) M:L ratio: 0.5:1; B) M:L ratio 1: 1 C) M:L ratio 2:1; [L] = 1 × 10^{-5} mol dm^{-3}.

Table 3: Experimental conditions for hydrogen peroxide and ascorbate assay carried out on hIAPP, hIAPP(H18A), rIAPP and their Cu(II) complex species reported in literature.

Assay	[Buffer][a]	pH	[Cu²⁺][a]	[hIAPP][a]	[rIAPP][a]	Fluorogenic probe[b]	Sensor	Ref.
Hydrogen peroxide	5×10^{-2} (PBS)	7.4	-	1×10^{-4}	-	DHPA	HRP	53
Hydrogen peroxide	5×10^{-2} (PBS)	7.4	-	-	1×10^{-4}	DHPA	HRP	53
Hydrogen peroxide	1×10^{-2} (HEPES)	7.4	1×10^{-5}	1×10^{-5}	-	DHPA	HRP	53
Hydrogen peroxide	1×10^{-2} (HEPES)	7.4	1×10^{-5}	-	1×10^{-4}	DHPA	HRP	53
Hydrogen peroxide	1.2×10^{-2} (PBS)	7.4	-	1×10^{-5}	-	H₂DCF	HRP	54
Hydrogen peroxide	1.2×10^{-2} (PBS)	7.4	2×10^{-5}	1×10^{-5}	-	H₂DCF	HRP	54
Hydrogen peroxide	5×10^{-2} (PBS)	7.4	-	1×10^{-6} (H18A)	-	DHPA	HRP	52
Hydrogen peroxide	5×10^{-2} (PBS)	7.4	1×10^{-5}	1×10^{-6} (H18A)	-	DHPA	HRP	52
Ascorbate	1×10^{-2} (PBS)	7.0	-	2×10^{-5}	-	-	-	48
Ascorbate	1×10^{-2} (PBS)	7.0	-	-	2×10^{-5}	-	-	48
Ascorbate	1×10^{-2} (PBS)	7.0	2×10^{-5}	2×10^{-5}	-	-	-	48
Ascorbate	1×10^{-2} (PBS)	7.0	2×10^{-5}	-	2×10^{-5}	-	-	48

[a] Concentrations are in mol dm^{-3}; [b] DHPA (Amplex red) = 10-acetyl-3,7-dihydroxyphenoxazine; H₂DFC = 2',7'-dichlorodihydrofluorescein diacetate; HRP = Horse Radish Peroxidase.

This behavior confirms the fluorescence results showing the Cu²⁺ inhibition ability of hIAPP fibril formation in the presence both of the same molar equivalents of the peptide and the metal ion[48] and of an excess of metal ion with respect to peptide.[46]

The toxicity of hIAPP has also been attributed to the oxidative stress caused by the production of H₂O₂ concomitant[52-53] or not [48] with the fibril formation both in absence or in presence of copper(II) ion. hIAPP, its point mutated (H18A) derivative and, in some case, rat IAPP,[48] produced small (sub-micromolar) amount of H₂O₂,[52-53] Fluorogenic probes as H₂DFC or Amplex Red have been employed they upon enzymatic oxidation by HRP showed fluorescing activity (see Table 3).[52-53]

Catalase addition at the end of the peptide incubation period or the inclusion of diethylenetriaminepentaacetic acid (DETAPAC) during peptide incubation blocked the oxidative signal, confirming the active role of H₂O₂ and suggesting the involvement of a redox-active metal ion, respectively.

This hIAPP ability to generate oxidative stress in cell-free conditions has been claimed [52-53] in analogy with Aβ findings that

suggested spontaneous peptide ROS generation.[80] This result, however, has successively been disputed.[81-82]

Furthermore, the presence of redox-active transition metal ions have been invoked to produce reactive oxygen species via Fenton reactions[83-86] and Huang et al. suggested that Cu²⁺-bound Aβ was capable of generating H₂O₂ without the presence of an additional reducing agent.[83-84]

However, subsequent studies induced the same laboratory to retract the previous results because the experiments to detect H₂O₂ were unreliable for the presence of tris(2-carboxyethyl)phosphine (TCEP), capable of acting as a reducing agent.[87]

This study highlighted the additional requirement of biological reductants (such as ascorbic acid, cholesterol, L-DOPA or dopamine) to act as substrates for the sequence of electron transfer reactions.[87-88]

Having in mind that similar artefactual oxidation reactions might affect the hIAPP induced oxidative stress, we started an accurate inspection of the experimental conditions reported in literature

(see Table 3) to identify possible sources both of redox active metal ions and of reducing agents.

Buettner findings showed that trace amounts of adventitious redox-active transition metals in buffer solutions served as catalysts for oxidative processes. He proved the catalytic role of copper trace in phosphate by ascorbate autoxidation in a quick and easy test.[89]

This literature finding together with the high concentration of phosphate buffer (5×10^{-2} mol dm^{-3}) used in all experiments carried out to determine H_2O_2 production by hIAPP (1×10^{-6} mol dm^{-3}), clearly indicate the origin of redox-active metal ion.

The stability constants here reported were again used to simulate the amount of copper(II) complexes with phosphate in comparison to metal complexes with the full length polypeptide. The results show that copper phosphate is present in different amount (see fig. 3S-4S) according to the diverse buffer/hIAPP ratios that mimic the experimental conditions reported in Table 3. [52-53]

The distribution diagram (Figure 4S), namely, shows that the [Cu(HPO$_4$)] formation results more favored at pH 7.4 with respect the copper-peptide complex species. In the presence of added Cu^{2+}, the copper bound to the phosphate is the main species (figure 5S).

To answer to the question of the main player of copper reduction, it has been need to hunt for it. H_2O_2 concentrations have been determined by means of Amplex Red and H_2DCF (Table 3), despite the demonstrated propensity of these probes to artefactual oxidation and self-generation of H_2O_2.[90] Limitations to the use of H_2DCF as a specific marker for H_2O_2 formation include stimulation of fluorescent DCF formation by redox-active metal ions as iron and copper.[91]

Peroxidases are also capable of promoting H_2DCF oxidation in the absence of H_2O_2,[92] thus it is reasonable to assume that HRP also affected the results summarized in Table 3.

The role played by the trace amount of copper in PBS, the fluorogenic probes and HRP suggests a possible explanation of the further finding that comparable levels ($1-6 \times 10^{-7}$ mol dm^{-3}) of H_2O_2 have been detected using different hIAPP concentrations, ranging from 2×10^{-5} mol dm^{-3} to 1×10^{-4} mol dm^{-3}.[48,52-53]

The speciation diagrams show (Figure 6S) that the [CuHPO$_4$] formation increases when the hIAPP concentration decreases, favoring the formation of the redox species that is responsible of H_2O_2 production.

The oxidative stress findings reported for rIAPP in the absence and presence of Cu^{2+} could be attributed to the artefactual oxidation reactions due both to the copper trace amount in phosphate and to the fluorogenic probes employed in the cell-free assay. The lower affinity for Cu^{2+} of rIAPP than hIAPP favors a higher formation of [CuHPO$_4$].[48]

The presence of reducing species causes the IAPP toxicity in cellular assays

Copper bound to hIAPP results protective by inhibiting activation of pro-apoptotic caspase-3 and stress-kinase signaling pathways in rat pancreatic insulinoma cells as well as in its native conformational state.[48]

Conversely, in the same cell lines, studies focused on the action mechanisms displayed that copper compounds increase hIAPP-induced cytotoxicity by facilitating apoptosis-promoting effect of hIAPP. Furthermore, Cu^{2+}-promoted ROS overproduction and mitochondrial disruption was proposed to be the main reason for the enhanced apoptosis.[49]

These findings are in contrast with the human IAPP ability to diminish the ability of glutathione to reduce copper and produce H_2O_2. This protective effect was much less apparent in the case of the other cellular reducing agent ascorbate; however, there was no further potentiation of H_2O_2 production in vitro by Cu^{2+} and either reductant.[48]

The simulation performed in the same conditions of biological assays (1:1 metal to ligand ratio) suggests that the protective effect is attributable to the chelating ability of the polypeptide as can be inferred by the distribution diagram (Figure 6S and 7S).[48] Caution is required to extrapolate the speciation data obtained in cell-free conditions to the complex cellular environment, but recent literature findings help to clarify the above-cited conflicting results. The N-terminal region of IAPP contains a conserved disulfide bond between cysteines at position 2 and 7, which is important to hIAPP's in vivo function and may play a role in in vitro aggregation.[93]

The importance of the disulfide bond in this region has been probed using a combination of ion mobility-based mass spectrometry experiments, molecular dynamics simulations, and high resolution atomic force microscopy imaging on the wild type 1-8 hIAPP fragment, a reduced fragment with no disulfide bond, and a fragment with both cysteines at positions 2 and 7 mutated to serine. The presence of the disulfide bond in the N-terminal fragment did not completely inhibit self-aggregation of the fragment, but reduction of the disulfide bond or its removal by mutation increased the rate of aggregation.[94]

This behavior has primarily been attributed to a significant reduction in intermolecular hydrogen bonds relative to the noncyclic peptides, suggesting that the disulfide bond may actually protect full-length hIAPP from amyloid formation.

To assess the apoptotic role of hIAPP, the INS-1 cellular assay have been carried out in the presence of mercaptoethanol; this reducing agent can reduce the disulfide bond of IAPP and the interaction of thiol groups with copper(II) ion can drive the oxidative stress responsible of IAPP toxicity.[49,95]

Conclusions

The synthesis of some hIAPP PEG-ylated peptide fragments encompassing the His 18 metal main binding site allowed us to determine the affinity and speciation of the different copper(II) complexes, mimicking the hIAPP behaviour. The accurate speciation contributed to assess the copper-IAPP binding details and to resolve the recent conflicting suggestions on the amino acid sequence involved in metal interaction.[41, 96] Taken together, our data indicate the involvement of the residues that precede His 18, favouring the amino acid peptide deprotonation towards the N-terminus.

Our speciation results clearly indicate that, at least in cell-free conditions, hIAPP toxicity cannot be attributed to production of oxidative stress. The knowledge of stability constants of copper(II) complexes with the hIAPP peptide fragment encompassing the histidine metal binding site, allow us to explain the role played by metal ion to decrease the formation of oligomeric species when the metal to polypeptide ratio increases.

Speciation also contributes to assess the sacrificial quenching of metal-catalyzed ROS by human hIAPP and copper's anti-apoptotic properties suggesting a novel and protective role for the copper-hIAPP complexes.

Experimental section

Materials. All N-fluorenylmethoxycarbonyl (Fmoc)-protected amino-acids, and 2-(1-H-benzotriazole-1-yl) -1,1,3,3-tetramethyluronium tetrafluoroborate (TBTU),); Fmoc- PAL-PEG resin were obtained from Novabiochem (Switzerland). N,N-Diisopropyl-ethylamine (DIEA), N,N-dimethylformamide (DMF, peptide synthesis grade) and 20% piperidine-DMF solution were from Merk. N-hydroxybenzotriazole (HOBT), triisopropylsilane (TIS), trifluoroacetic acid (TFA) were purchased from Sigma/Aldrich. All the other chemicals were of the highest available grade and were used without further purification.

Peptide synthesis and purification. The peptides Ac-Peg$_{11}$-VHSSNNFGAILSS-NH$_2$ (Peg-hIAPP(17-29)) and Ac-VHSSNNLGPVLPP-NH$_2$ (rIAPP(17-29)R18H) were synthesized as previously reported.[65-66] The peptide Ac-Peg$_4$-NFLVHSS-NH$_2$ (Peg-hIAPP(14-22)) was purchased by CASLO (Lyngby, Danmark). The peptide Ac-NFLVHSSNN-NH$_2$ (hIAPP(14-22)) was assembled using the solid phase peptide synthesis strategy on a Biotage initiator+ AlstraTM fully automated microwave peptide synthesizer. Syntheses were carried out on TGR resin (0.25 mmol/g) on 0.11 mmol scale using a 30 mL reactor vial. Fmoc deprotection steps were performed at room temperature with piperidine/DMF solution for 15 minutes. Peptide couplings were performed using 5 equivalent of amino acid, 5 equivalent of HOBT/TBTU/DIPEA in DMF. A coupling time of 10 minutes at room temperature was employed. The N-terminal amino group was acetylated with a solution of acetic anhydride (6% v/v), DIPEA (5% v/v) in DMF. Other experimental details have already been reported.[65-66] Peptide was purified by means of a preparative reversed-phase high-performance liquid chromatography (rp-HPLC), on a Varian PrepStar 200 model SD-1 chromatography system. Analytical rp-HPLC analysis were performed using a Agilent 1200 series instrument, using gradient elution with solvent A (0.1% TFA in water) and B (0.1% TFA in acetonitrile) on a Vydac C$_{18}$ 250 × 4.6 mm (300 Å pore size, 5 μm particle size) column, at a flow rate of 1 mL/min. The peptide was eluted according to the following protocol: from 0 to 5 minutes isocratic gradient in 15% B, then linear gradient from 15 to 25% B over 20 min. Finally isocratic gradient in 15% B from 25 to 30 minutes. The peptide was characterized by means of Electron Spray Ionization Mass Spectrometry (ESI-MS).

Ac-NFLVHSSNN-NH$_2$ (hIAPP(14-22)). Yield: 60% (R$_t$ = 16.15 min). ESI-MS m/z calc for C$_{46}$H$_{69}$N$_{15}$O$_{15}$ = 1072.49; found (M+H)$^+$ 1073.3 (M+2H)$^{2+}$ 536.8.
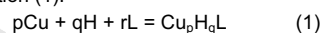
Potentiometric titrations. Potentiometric titrations were performed with two home-assembled fully automated apparatus sets (Metrohm E654 pH-meter, combined micro pH glass electrode, Orion 9103SC, Hamilton digital dispenser, Model 665) controlled by the appropriate software set up in our laboratory. The titration cell (2.5 ml) was thermostated at 298.0 ± 0.2 K, and all solutions were kept under an atmosphere of argon, which was bubbled through a solution having the same ionic strength and temperature as the measuring cell. KOH solutions (0.1 mol dm^{-3}) were added through a Hamilton buret equipped with 1 cm^3 syringes. Solutions ionic strength was adjusted to 0.1 mol dm^{-3} (KNO$_3$). To determine the stability constants, solutions of the ligands (protonation constants) or the

ligands with Cu^{2+} (copper(II) complex constants) were titrated by using 0.1 mol dm^{-3} potassium hydroxide. The peptide concentration used in the protonation and complexation experiments was 1.0 x 10^{-3} mol dm^{-3} for Peg-hIAPP(17-29) and Peg-hIAPP(14-22) and in the range from 1.0 to 2.0 x 10^{-3} mol dm^{-3} for rIAPP(17-29)R18H. A minimum of four independent runs were performed to determine the protonation constants, while four independent experiments were run for the copper(II) complexation constants. The initial pH was always adjusted to 2.3. To avoid systematic errors and verify reproducibility, the EMF values of each experiment were taken at different time intervals. Other details are reported elsewhere.[97] To obtain protonation and complexation constants, the potentiometric data were refined using the HYPERQUAD program,[98] which minimizes the error square sum of the measured electrode potentials through a nonlinear iterative refinement of the sum of the squared residuals, U, and also allows for the simultaneous refinement of data from different titrations:

$$U = \Sigma(E_{exp} - E_{calc})^2$$

E$_{exp}$ and E$_{calc}$ are the experimental and calculated electrode potentials, respectively. Errors in stability constant values are reported as three times standard deviations.

The formation reaction equilibria of ligands with protons and copper(II) ions are given in Equation (1):

$$pCu + qH + rL = Cu_pH_qL \qquad (1)$$

in which L are the peptides here studied. The stability constant β_{pqr} is defined in Equation (2):

$$\beta_{pqr} = [Cu_pH_qL_r] / [Cu]^p \times [H]^q \times [L]^r \qquad (2)$$

The species distribution as a function of the pH was obtained by using the computer program Hyss.[99]

Spectroscopic studies: *UV-vis measurements.* UV-vis spectra were recorded at 25°C, by using an Agilent 8453 or a Varian Cary 500 spectrophotometer. The concentrations of the peptides and copper(II) used to record absorption spectra were the same as those for the potentiometric titrations. Combined spectroscopic and potentiometric metal-complex titrations were performed into a 3 ml quartz cUVette with a 1 cm path length to get the spectrum in the visible region at each pH value simultaneously. These experiments were replicated at least three times for each copper-peptide system. Spectroscopic data were processed by using the HYPERQUAD program.[98]

CD measurements. CD spectra were obtained at 25° C under a constant flow of nitrogen on a Jasco model 810 spectropolarimeter at a scan rate of 50 nm min^{-1} and a resolution of 0.1 nm. The path lengths were 1 cm, in the 190-800 nm range. The spectra were recorded as an average of 10 scans in the UV region and 3 scans in the Vis region, respectively. Calibration of the instrument was performed with a 0.06% solution of ammonium camphorsulfonate in water. The CD spectra of the copper(II) complexes on varying the solution pH were obtained in 190-260, 240-400 and 300-800 nm wavelength regions. All the solutions were freshly prepared using double distilled water. The copper(II) ion and peptide concentrations used for the acquisition of the CD spectra in the visible region were identical to those used in the potentiometric titrations. CD spectra in the region 240-400 were acquired by using copper(II) ion and peptide concentrations of 5.0 × 10^{-4} mol dm^{-3}. The results are reported as $\Delta\varepsilon$ (molar dichroic coefficient) in M^{-1} cm^{-1}.

EPR measurements. A Bruker Elexsys E500 CW-EPR spectrometer driven by a PC running XEpr program under Linux and equipped with a Super-X microwave bridge, operating at 9.3-9.5 GHz, and a SHQE cavity was used throughout this work. All EPR spectra of frozen solutions of copper(II) complexes were recorded at 150 K by means of a ER4131VT variable temperature apparatus. EPR magnetic parameters were obtained directly from the experimental EPR spectra, always calculating them from

the 2nd and the 3rd line to get rid of second order effects. Instrumental settings of EPR spectra recordings of the copper(II)-peptide complexes were as follow: number of scans 1–5; microwave frequency 9.344–9.376 GHz; modulation frequency 100 kHz; modulation amplitude 0.2-0.6 mT; time constant 164-327 ms; sweep time 2.8 min; microwave power 20-40 mW; receiver gain 1×10^4-2×10^5. Copper(II) complexes were prepared by addition of the appropriate amount of isotopically pure copper, taken from a ^{63}Cu(NO$_3$)$_2$ 0.05 mol dm^{-3} solution, to the peptide solution. Copper(II) complexes solutions were prepared in 10% methanol-water mixture.
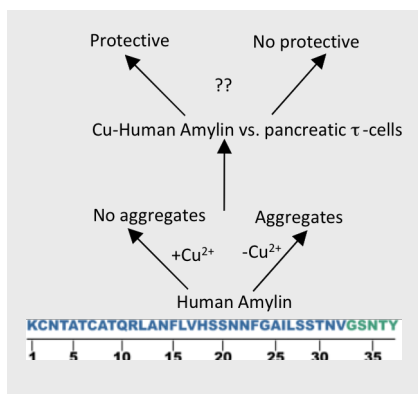
[1] P. H. Weinreb, W. Zhen, A. W. Poon, K. A. Conway, P. T. Lansbury Jr., *Biochemistry* **1996**, *35* 13709-13715.
[2] P. E. Wright, H. J. Dyson, *J. Mol. Biol.* **1999**, *293*, 321-331.
[3] A. K. Dunker, J. D. Lawson, C. J. Brown, R. M. Williams, P. Romero, J. S. Oh, C. J. Oldfield, A. M. Campen, C. M. Ratliff, K. W. Hipps, J. Ausio, M. S. Nissen, R. Reeves, C. Kang, C. R. Kissinger, R. W. Bailey, M. D. Griswold, W. Chiu, E. C. Garner, Z. Obradovic, *J. Mol. Graphics Modell.* **2001**, *19*, 26-59.
[4] P. E. Wright, H. J. Dyson, *Curr. Opin. Struct. Biol.* **2009**, *19*, 31-38.
[5] K. Van Roey, T. J. Gibson, N. E. Davey, *Curr. Opin. Struct. Biol.* **2012**, *22*, 378-385.
[6] V. N. UVersky, *Biochim. Biophys. Acta* **2013**, *1834*, 932-951.
[7] P. Tompa, N. E. Davey, T .J. Gibson, M. M. Babu, *Mol. Cell* **2014**, *55* 161-165.
[8] A. K. Dunker, V. N. UVersky, *Nature Chem. Biol.* **2008**, *4*, 229-230.
[9] H. J. Dyson, P. E. Wright, *Nature Rev. Mol. Cell Biol.* **2005**, *6*, 197-208.
[10] F. Chiti, C. M. Dobson, *Annu. Rev. Biochem.* **2006**, *75*, 333-366.
[11] A. Iram, A. Naeem, *Cell Biochem. Biophys.* **2014**, *70*, 51-61.
[12] G. T. Westermark, M. Fandrich, P. Westermark, *Ann. Rev. Pathol.* **2015**, *10*, 321-344.
[13] G. T. Westermark, P. Westermark, *Curr. Protein Pept. Sci.* **2013**, *14*, 330-337.
[14] G. J. Cooper, A. C. Willis, A. Clark, R. C. Turner, R. B. Sim, K. B. Reid, *Proc. Natl. Acad. Sci. U.S.A.* **1987**, *84*, 8628-8632.
[15] A. Clark, C. E. Lewis, A. C. Willis, G. J. S. Cooper, J. F. Morris, K. B. M. Reid, R. C. Turner, *Lancet* **1987**, *2*, 231-234
[16] P. Westermark, A. Andeersson, G. T. Westermark, *Physiol. Rev.* **2011**, *91*, 795-826.
[17] C. Röcken, R. P. Linke, W. Saeger, *Virchows Arch A Pathol Anat Histopathol.* **1992**, *421*, 339-344.
[18] R. P. Nanga, J. R. Brender, J. Xu, G. Veglia, A. Ramamoorthy, *Biochemistry* **2008**, *47*, 12689-12697.
[19] G. Liang, J. Zhao, X. Yu, J. Zheng, *Biochemistry* **2013**, *52*, 1089-1100.
[20] N. F. Dupuis, C. Wu, J.-E. Shea, M. T. Bowers, *J. Am. Chem. Soc.* **2009**, *131* 18283-18292.
[21] A. S. Reddy, L. Wang, S. Singh, Y. L. Ling, L. Buchanan, M. T. Zanni, J. L. Skinner, J. J. de Pablo, *Biophys. J.* **2010**, *99*, 2208-2216.
[22] N. F. Dupuis, C. Wu, J.-E. Shea, M. T. Bowers, *J. Am. Chem. Soc.* **2011**, *133*, 7240-7243.
[23] S. Singh, C.-C. Chiu, A. S. Reddy, J. J. de Pablo, *J. Chem. Phys.* **2013**, *138*, 155101-15510.
[24] C.-C. Chiu, S. Singh, J. J. de Pablo, *Biophys. J.* **2013**, *105*, 1227-1235.
[25] C. Wu, J.-E. Shea, *PLoS Comput. Biol.* **2013**, *9*, e1003211
[26] J. D. Knight, J. A. Hebda, A. D. Miranker, *Biochemistry* **2006**, *45*, 9496-9508.
[27] R. P. R. Nanga, J. R. Brender, J. Xu, K. Hartman, V. Subramanian, A. Ramamoorthy, *J. Am. Chem. Soc.* **2009**, *131*, 8252-8261.
[28] S. M. Patil, S. Xu, S. R. Sheftic, A. T. Alexandrescu, *J. Biol. Chem.* **2009**, *284* 11982-11991.
[29] J. A.Williamson, A. D. Miranker, *Protein Sci.* **2007**, *16*, 110-117.
[30] C. Betsholtz, L. Christmansson, U. Engstroem, S. Frederik, J. Viveka, H. Kenneth, P. Westermark, *FEBS Lett.* **1989**, *251*, 261-264.
[31] P. Westermark, U. Engstroem, K. H. Johnson, G. T. Westermark, C. Betsholtz, *Proc. Natl. Acad. Sci. U.S.A.*, **1990**, *87*, 5036-5040.
[32] E. T. A. S. Jaikaran, C. E. Higham, L. C. Serpell, J. Zurdo, M. Gross, A. Clark, P.E. Fraser, *J. Mol. Biol.* **2001**, *308*, 515-525.
[33] A. V. Kajava, U. Aebi, A. C. Steven, *J. Mol. Biol.* **2005**, *348*, 247-252.
[34] S. Luca, W. M. Yau, R. Leapman, R. Tycko, *Biochemistry* **2007**, *46*, 13505-13522.
[35] K. Pillay, P. Govender, *BioMed Research International* **2013**, Article ID 826706, 17 pages, doi:10.1155/2013/826706.
[36] E. Jaikaran, A. Clark, *Biochim. Biophys. Acta* **2001**, *1537*, 179-203.
[37] A. Abedini, D. P. Raleigh, *Biochemistry* **2005**, *44*, 16284-16291.
[38] Y. Li, W. Xu, Y. Mu, J. Z. Zhang, *J. Chem. Phys.* **2013**, *139*, 055102.
[39] J. R. Brender, K. Hartman, K. R. Reid, R. T. Kennedy, A. Ramamoorthy, *Biochemistry* **2008**, *47*, 12680-12688.
[40] L. Rivillas-Acevedo, C. Sánchez-López, C. Amero, L. Quintanar, *Inorg. Chem.* **2015**, *54*, 3788-3796.
[41] A. Sinopoli, A. Magrì, D. Milardi, M. Pappalardo, P. Pucci, A. Flagiello, J. J. Titman, V. G. Nicoletti, G. Caruso, G. Pappalardo, G. Grasso, *Metallomics* **2014**, *6*, 1841-1852.
[42] F. Bellia, G. Grasso, *J. Mass Spectrom.* **2014**, *49*, 274-279.
[43] J. R. Brender, J. Krishnamoorthy, G. M. Messina, A. Deb, S. Vivekanandan, C. La Rosa, J. E. A. Penner-Hahn, A. Ramamoorthy, *Chem. Commun.* **2013**, *49*, 3339-3341.
[44] S. Salamekh, J. R. Brender, S. J. Hyung, R. P. Nanga, S. Vivekanandan, B. T. Ruotolo, A. Ramamoorthy, *J. Mol. Biol.* **2011**, *410*, 294-306.
[45] J. R. Brender, K. Hartman, R. P. Nanga, N. Popovych, R. de la Salud Bea, S. Vivekanandan, E. N. Marsh, A. Ramamoorthy, *J. Am. Chem. Soc.* **2010**, *132*, 8973-8983.
[46] B. Ward, K. Walker, C. Exley, *J. Inorg. Biochem.* **2008**, *102*, 371-375.
[47] Y. Hirakura, W. W. Yiu, A. Yamamoto, B. L. Kagan, *Amyloid* **2000**, *7*, 194-199.
[48] E. C. Lee, E. Ha, S. Singh, L. Legesse, S. Ahmad, E. Karnaukhova, R. P. Donaldson, A. M. Jeremic, *Phys. Chem. Chem. Phys.* **2013**, *15*, 12558-12571.
[49] L. Ma, X. Li, Y. Wang, W. Zheng, T. Chen, *J. Inorg. Biochem.* **2014**, *140*, 143-152.
[50] M. J. Kim, H. T. Kim, Eur. *J. Mass Spectrom.* **2012**, *18*, 51-58.
[51] S. M. Mirhashemi, M. E. Shahabaddin, *J. Pak. J. Biol. Sci.* **2011**, *14*, 288-292.
[52] A. Masad, B. J. Tabner; J. Mayes, D. Allsop, *Free Radic. Biol. Med.* **2011**, *51*, 869-875.
[53] A. Masad, L. Hayes, B. J. Tabner, S.Turnbull, L. J. Cooper, N. J. Fullwood, M. J. German, F. Kametani, O. M. El-Agnaf, D. Allsop, *FEBS Lett.* **2007**, *581*, 3489-3493.
[54] Y. P. Yu, P. Lei, J. Hu, W. H. Wu, Y. F. Zhao, Y. M. Li, *Chem. Commun.* **2010**, *46*, 6909-6911.
[55] P. Westermark, Z. C. Li, G. T. Westermark, A. Leckstrom, D. F. Steiner, *FEBS Lett.* **1996**, *379*, 203-206.
[56] K. Lemaire, M. A. Ravier, A. Schraenen, J. W. M. Creemers, R. Van de Plas, M. Granvik, L. Van Lommel, E. Waelkens, F. Chimienti, G. A. Rutter, P. Gilon, P. A. in't Veld, F. C. Schuit, *Proc. Natl. Acad. Sci. U. S. A.* **2009**, *106*, 14872-14877.
[57] T. Naka, H. Kaneto, N. Katakami, T. A. Matsuoka, A. Harada, Y. Yamasaki, M. Matsuhisa, I. Shimomura, *Endocr. J.* **2013**, *60*, 393-396.
[58] T. Naka, H. Kaneto, T. Miyatsuka, K. Yamamoto, K, Yoshiuchi, Y. Yamasaki, I. Shimomura, T. A. Matsuoka, M. Matsuhisa, *Endocr. J.* **2009**, *56*, 699-706.
[59] J. Y. Uriu-Adams, R. B. Rucker, J. F. Commisso, C. L. Keen, *J. Nutr. Biochem.* **2005**, *16*, 312-320.
[60] C. E. E. House, T. Patel, L. Wu, P. E. Fraser, *J. Inorg. Biochem.* **2010**, *104*, 1125-1129.
[61] S. Janciauskiene, B. Ahren, *Biochem. Biophys. Res. Commun.* **2000**, *267*, 619-625.
[62] C. Exley, M. Mold, E. Shardlow, B. Shuker, B. Ikpe, L. Wu, P. E. Fraser, *J. Diabetes Res. Clin. Metab.* **2012**, *1*, 1-6.

[63] H. Li, E. Ha, R. P. Donaldson, A. M. Jeremic, A. Vertes, *Anal. Chem.* **2015**, *87*, 9829-9837.

[64] P. Nedumpully-Govindan, Y. Yang, R. Andorfer, W. Cao, F. Ding, *Biochemistry* **2015**, *54*, 7335-7344.

[65] G. Pappalardo, D. Milardi, A. Magrì, F. Attanasio, G. Impellizzeri, C. La Rosa, D. Grasso, E. Rizzarelli, *Chem.-Eur. J.* **2007**, *13*, 10204-10215.

[66] A. Mazzaglia, N. Micali, L. Monsù-Scolaro, F. Attanasio, A. Magrì, G. Pappalardo, V. Villari, *J. Phys. Chem. B* **2010**, *114*, 705-713

[67] M.F. Tomasello, A. Sinopoli, F. Attanasio, M. L. Giuffrida, T. Campagna, D. Milardi, G. Pappalardo, *Eur. J. Med. Chem.* **2014**, *81*, 442-455.

[68] M. Mylonas, J.C. Plakatouras, N. Hadjiliadis, A. Krezel, W. Bal, *Inorg. Chim. Acta* **2002**, *339*, 60-70.

[69] I. Sovago, K. Osz, *Dalton Trans.* **2006**, 3841-3854.

[70] D. La Mendola, A. Magrì, Ö. Hansson, R. P. Bonomo, E. Rizzarelli *J. Inorg. Biochem.* **2009**, *103*, 758-765.

[71] A. A. Adzhubei, M. J. E. Sternberg, A. A. Makarov, *J. Mol. Biol.* **2013**, *425*, 2100-2132.

[72] D. La Mendola, R.P. Bonomo, G. Impellizzeri, G. Maccarrone, G. Pappalardo, A. Pietropaolo, E. Rizzarelli, V. Zito, *J. Biol. Inorg. Chem.* **2005**, *10*, 463-475.

[73] H. Kozlowski, W. Bal, M. Dyba and T. Kowalik-Jankowska, *Coord. Chem. Rev.* **1999**, *184*, 319-346.

[74] M. Luczkowski, H. Koszlowski, M. Stawikowski, K. Rolka, E. Gaggelli, D. Valensin, G. Valensin, *J. Chem. Soc. Dalton Trans.* **2002**, 2269-2274.

[75] D. La Mendola, A. Magrì, L. I. Vagliasindi, Ö. Hansson, R. P. Bonomo, E. Rizzarelli, *Dalton Trans.* **2010**, 10678-10684.

[76] S. Pizzanelli, C. Forte, C. Pinzino, A. Magrì, D. La Mendola, *Phys. Chem. Chem. Phys.* **2016**, *18*, 3982-3994.

[77] A. Magrì, F. D'Alessandro, D. A Distefano, T. Campagna, G. Pappalardo, G. Impellizzeri, D. La Mendola, *J. Inorg. Biochem.* **2012,** *113*, 15-24

[78] S. Zhang, H. Liu, G.V Amarsingh, C.C H Cheung, S. Hogl, U. Narayanan, L. Zhang, S. McHarg, J. Xu, D. Gong, J. Kennedy, B. Barry, Y. S. Choong, A. R J Phillips, G. J S Cooper, *Cardiovasc. Diabetol.* **2014**, 13, 100.

[79] M. F. Tomasello, A. Sinopoli, G. Pappalardo, *J. Diabetes Res.* **2015**, Article ID 918573, 15 pages. dx.doi.org/10.1155/2015/918573.

[80] K. Hensley, J. M. Carney, M. P. Mattson, M. Aksenova, M. Harris, J. F. Wu, R. A. Floyd, D. A. Butterfield, *Proc. Natl. Acad. Sci. U.S.A.* **1994***, 91*, 3270-3274.

[81] S. I. Dikalov, M. P. Vitek, K. R. Maples, R. P. Mason, *J. Biol. Chem.* **1999***, 274*, 9392-9399.

[82] S. Turnbull, B. J. Tabner, O. M. El-Agnaf, L. J. Twyman, D. Allsop, *Free Radic. Biol. Med.* **2001**, *30*, 1154-1162.

[83] X. Huang, C. S. Atwood, M. A. Hartshorn, G. Multhaup, L. E. Goldstein, R. C. Scarpa, M. P. Cuajungco, D. N. Gray, J. Lim, R. D. Moir, R. E. Tanzi, A. I. Bush, *Biochemistry* **1999,** *38*, 7609-7616.

[84] X. Huang, M. P. Cuajungco, C. S. Atwood, M. A. Hartshorn, J. D. Tyndall, G. R. Hanson, K. C. Stokes, M. Leopold, G. Multhaup, L. E. Goldstein, R. C. Scarpa, A. J. Saunders, J. Lim, R. D. Moir, C. Glabe, E. F. Bowden, C. L. Masters, D. P. Fairlie, R. E. Tanzi, A. I. Bush, *J. Biol. Chem.* **1999**, *274*, 37111-37116.

[85] B. J. Tabner, S. Turnbull, O. M. El-Agnaf, D. Allsop, *Free Radic. Biol. Med.* **2002**, *32*, 1076-1083.

[86] S. C. Bondy, S. X. Guo-Ross, A. T. Truong, *Brain Res.* **1998***, 799*, 91-96.

[87] C. Opazo, X. Huang, R. A. Cherny, R. D. Moir, A. E. Roher, A. R. White, R. Cappai, C. L. Masters, R. E. Tanzi, N. C. Inestrosa, A. I. Bush, *J. Biol. Chem.* **2002**, *277*, 40302-40308.

[88] K. J. Barnham, F. Haeffner, G. D. Ciccotosto, C. C. Curtain, D. Tew, C. Mavros, K. Beyreuther, D. Carrington, C. L. Masters, R. A. Cherny, R. Cappai, A. I. Bush, *FASEB J.* **2004***, 18*, 1427-1429.

[89] G. R. Buettner, *J. Biochem. Biophys. Methods* **1988**, *16*, 27-40.

[90] D. Debski, R. Smulik, J. Zielonka, B. Michałowski, M. Jakubowska, K. Dębowska, J. Adamus, A. Marcinek, B. Kalyanaraman, A. Sikora, *Free Rad. Biol. Med.* **2016**, *95*, 323-332.

[91] M. B. Grisham, in *Redox Biochemistry*, (Ed. R. Banerjee), Wiley and Sons, Inc., Hoboken, New Jersey, USA, **2008,** pp. 272-284.

[92] T. V. Votyakova, I. J. Reynolds, *Arch. Biochem. Bioph.* **2004**, *431*, 138-144.

[93] L. Khemtémourian M. F. Engel, J. A. Kruijtzer, J. W. Höppener, R. M. Liskamp, J. A. Killian, *Eur. Biophys. J.* **2010**, *39*, 1359-64.

[94] A. I. Ilitchev, M. J. Giammona, T. D. Do, A.G. Wong, S. K. Buratto, J. Emma Shea, D. P. Raleigh, M. T. Bowers, *J. Am. Soc. Mass Spectrom*. **2016**, 138, 549-557.

[95] V. Wineman-Fisher, L. Tudorachi, E. Nissim, Y. Miller, *Phys. Chem. Chem. Phys.* **2016**, *18*, 12438-12442.

[96] M. Rowinska-Zyrek, *Dalton Trans*, **2016**, *45*, 8099-8106.

[97] D. La Mendola, A. Magrì, T. Campagna, M. A. Campitiello, L. Raiola, C. Isernia, Ö. Hansson, R. P Bonomo, E. Rizzarelli, *Chemistry Eur.-J.*, **2010**, *16*, 6212-6223.

[98] P. Gans, A. Sabatini, A. Vacca, *Talanta* **1996**, *43*, 1739-1753.

[99] L. Alderighi, P. Gans, A. Ienco, D. Peters, A. Sabatini, A. Vacca, *Coord. Chem. Rev.* **1999**, *184*, 311-318.

Entry for the Table of Contents

FULL PAPER

Cu-hIAPP speciation by potentiometry unveils: i) the protective role played by increased Cu^{2+} amount on the hIAPP fibrillary aggregation; ii) the effect of adventitious trace of Cu^{2+} present in buffers iii) a reducing fluorogenic probe on H_2O_2 production attributed to the polypeptide alone.

Antonio Magrì*, Diego La Mendola,* Vincenzo G. Nicoletti, Giuseppe Pappalardo, Enrico Rizzarelli…

Page No. – Page No.

New insights in copper binding to human islet amyloid: the contribution of metal complex speciation to reveal the polypeptide toxicity